J|A|C|S COMMUNICATIONS

Published on Web 01/13/2009

Nanostructure and Hydrogen Spillover of Bridged Metal-Organic Frameworks

Cheng-Si Tsao,*,† Ming-Sheng Yu,† Cheng-Yu Wang,† Pin-Yen Liao,† Hsin-Lung Chen,‡ U-Ser Jeng,§ Yi-Ren Tzeng,† Tsui-Yun Chung,† and Hsiu-Chu Wu†

Institute of Nuclear Energy Research, Longtan 32546, Taiwan, Department of Chemical Engineering, National Tsinghua University, Hsinchu 30076, Taiwan, and National Synchrotron Radiation Research Center, Hsinchu 30076, Taiwan

Received April 15, 2008; Revised Manuscript Received January 3, 2009; E-mail: cstsao@iner.gov.tw

Hydrogen storage is one of the main challenges of the hydrogen economy and one of the bottlenecks to commercializing fuel-cell vehicles. New porous metal-organic frameworks (MOFs) have been identified as promising candidates for hydrogen storage.[1−3] The well-known MOF-5 was recently reported to have a saturated hydrogen uptake of ∼5 wt % at 77 K.[3] However, according to the U.S. Department of Energy (DOE) on-board criteria, the hydrogen uptake procedure must be reversible at ambient temperatures. The hydrogen uptake at room temperature (RT) for MOF-5 exhibited low values of 0.28 wt % at 6.5 MPa[3] and ∼0.4 wt % at 10 MPa.[4,5] Recently, Yang's group used secondary spillover on the MOFs as a novel approach to significantly enhance their reversible RT hydrogen uptake up to 4 wt % at 10 MPa,[5] a level which the currently available microporous materials cannot achieve via H_2 physisorption under the same conditions.

In the hydrogen spillover process, the adsorption/desorption of spiltover hydrogen atoms instead of H_2 occurs in the MOF (as the secondary receptor) mixed with a small amount of a carbon-supported Pt catalyst (as the primary spillover source), which can dissociate hydrogen molecules.[4,5] The dissociated atomic hydrogen migrates from the Pt surface to the carbon support (so-called primary spillover) and then moves to the MOF (secondary spillover). However, the mechanistic details of atomic hydrogen spillover are poorly understood.[6−8] The adsorption sites, space, diffusion process, and overall behavior of the H atoms in the spillover system are entirely different from those of H_2 physisorption; furthermore because they are largely favorable to RT hydrogen storage, they form an interesting and challenging scope of research. Currently, the understanding of the transport of spiltover hydrogen atoms is limited to the surface diffusion processes both within the carbon support and within the high-capacity MOF receptor. There is a general lack of knowledge regarding the correlation of the hydrogen uptake via spillover to the structures, such as the pore network, specific surface area (SSA), and lattice defects.

The present study demonstrates that RT hydrogen uptake via bridged spillover is mainly governed by the imperfect lattice structure (including the structural defects) and pore network in real MOF crystals. The hydrogen uptake can be further enhanced up to ∼1.8 times (at 6.9 MPa) higher than that reported by Yang et al.,[5] regardless of the measured specific surface area of the MOF, by tuning the synthesis factors. The special 3-D open pore network in the synthesized MOF crystal is related to the migration of atomic hydrogen and its presence facilitates the adsorption via spillover. A relationship among the synthesis conditions, structural characteristics, and hydrogen uptake via spillover in the bridged MOF as a conceptual breakthrough will also be proposed herein to provide an approach to optimizing the reversible RT hydrogen uptake.

Previous structural investigations of the involved materials focused on the Pt catalyst.[7−9] Three different carbon-supported Pt catalysts were selected in our bridged IRMOF-8 system to quantitatively study the effect of both the Pt and carbon structures on the RT hydrogen uptake via bridged spillover. Anomalous small-angle X-ray scattering (ASAXS)[10a,b] with two synchrotron energies was employed to simultaneously resolve the structural characteristics of the Pt particle and carbon support. Prepared IRMOF-8 crystals with different lattice defects, SSA values, and pore network structures were investigated here for the first time by SAXS and powder X-ray diffraction (XRD).[10c]

The IRMOF-8 crystals whose structures were to be characterized by XRD and N_2 sorption isotherm analysis were prepared on the basis of the procedure reported by Yaghi.[11] The synthesized IRMOF-8 crystals, which had a broad range of Brunauer−Emmet−Teller (BET) SSA values, were divided into three categories, denoted as M_SC1 (SSA: ∼1400 m^2/g; typical IRMOF-8),[2a] M_SC2 (SSA: ∼900 m^2/g; obtained by lowering the cooling rate), and M_SC3 (SSA: ∼400 m^2/g; obtained by an extended heating time with a scaled-up amount) (Supporting Information). The bridged IRMOF-8 samples were subsequently prepared according to Yang's procedure,[6] including the use of commercial 5 wt % Pt supported on active carbon (Pt/AC). The hydrogen storage measurement for a selected bridged M_SC1 sample (denoted as INER-SwRI) was performed independently at the South West Research Institute (SWRI), for a cross-check of our high-pressure thermal gravimetric analysis (TGA).

The measured RT hydrogen uptake of the INER-SWRI sample was reported by the DOE hydrogen program,[12] which also reproduced the same result as Yang et al.,[5,13] as shown in Figure 1. The regular measurement procedure took several hours to over one day, according to the rate acceptance criteria. Our bridged IRMOF-8 samples were found to have much slower adsorption kinetics than the samples reported by Yang et al.,[8] as shown in Figure 2. In this case, the equilibrium adsorption amount was achieved by continuing the TGA measurement for up to 72 h. It can be seen in Figure 1 that the hydrogen uptake of the bridged M_SC1 sample obtained by our regular TGA measurement at RT and 6.9 MPa was confirmed by its agreement with the data of the INER-SWRI sample. Moreover, the hydrogen uptakes of the bridged M_SC2 and 3 samples measured at RT and 6.9 MPa reached up to 4.2 wt %, which is much higher than that (∼2.6 wt %) of the materials reported by Yang et al.[5,13] under the same measurement conditions. Additionally, their corresponding equilibrium adsorption values were enhanced by up to 4.7 wt % at 6.9 MPa. It should be noted that the high RT hydrogen uptakes are not related to the measured SSA values of IRMOF-8 but can be

† Institute of Nuclear Energy Research.
‡ National Tsinghua University.
§ National Synchrotron Radiation Research Center.

10.1021/ja802741b CCC: $40.75

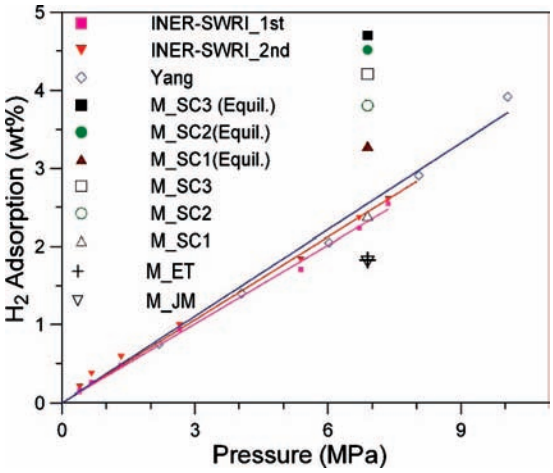

Figure 1. Hydrogen storage capacities at RT and 6.9 MPa for the bridged IRMOF-8 samples (both regular and equilibrium TGA measurements) in comparison to the high-pressure sorption isotherm analysis at RT, as measured by SWRI (twice), and Yang's result.

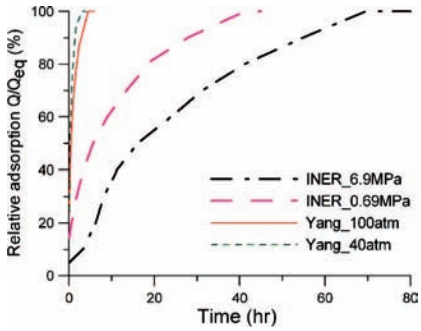

Figure 2. Comparison of pressure-dependent RT hydrogen adsorption rates of different bridged IRMOF-8 samples. Q_{eq} is the equilibrium adsorption amount at the prescribed pressure. The relative adsorption is equivalent to the percent toward completion.

attributed to differences in the structural defects (at the lattice scale) and the mesopore network of the real IRMOF-8 crystals (to be discussed later). Apparently, the maximum theoretical storage[5] (at least 6.5 wt %) can be expected to occur at 10 MPa or more. The desorption of all the samples was rapid, and the equilibrium value was reached within 20 h, indicating that adsorption and desorption processes might proceed via different reaction pathways.

The pore quality of the IRMOF-8 sample studied herein is very similar to that of the imperfect MOF-5 crystals reported previously,[14,15] which contain a partially collapsed framework. The amount of the produced structural defects in the lattice (i.e., the Zn−O species in the nanopores and lattice interpenetration as the minor phase) increases in order from M_SC1 to M_SC3, as revealed by the differences in peak splitting and relative peak intensities in the powder XRD pattern (Figure 3). These results consistently support the fact that the BET SSA value measured by the nitrogen sorption isotherm at 77 K is significantly reduced from ~1400 to ~400 m^2/g (from M_SC1 to M_SC3) because of the different degrees of blockage of the lattice defects acting as a diffusion hindrance to nitrogen molecules. In the present study, the diffusion of the spiltover H atoms is less limited in the collapsed framework structure than that of the H molecules.

Instead of the usual BET SSA, the RT hydrogen storage can be appropriately evaluated by the accessible surface area[16] (ASA) calculated geometrically from the real MOF crystal structure at the scale of a hydrogen atom. For clarity of discussion, we first consider

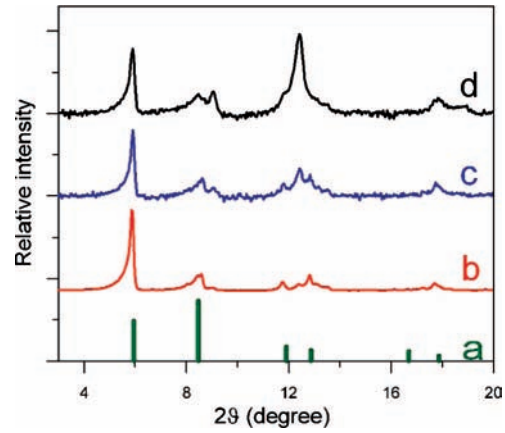

Figure 3. Powder XRD patterns of M_SC1 (b), M_SC2 (c), and M_SC3 (d) IRMOF-8 crystals compared to that from Yaghi's patent in the form of a bar chart (a).

the ASA, excluding any inclusion defects in the cavities (defined as ASA_L). It can be imagined that several collapsed frameworks, consisting of a high density of structural defects (associated with the pore-filling effect), may easily form a closed 3-D network. As the morphology of the IRMOF-8 synthesized here is polycrystal-like, such a network can be viewed as the grain boundary of the subgrain-like regions in the system. The ASA_L is still high within each nanometer-scale subgrain-like region. However, the high density of structural defects concentrating between the subgrain blocks the atomic hydrogen from diffusing into the subgrain region, making these zones inaccessible to atomic hydrogen. As a result, the ASA_L for atomic hydrogen and the BET SSA is greatly reduced.

On the basis of the above discussion, the increasing degree of the lattice defects from M_SC1 to M_SC3 should tend to exert a negative effect on the ASA_L and BET SSA, due to the increased number of isolated subgrains or the increased spatial density of lattice defects. However, the resultant 3-D mesopore network, with a higher openness and fine branch channels (to be shown later), breaks the boundaries and provides effective paths of surface diffusion for atomic hydrogen to accessible sites throughout the entire MOF crystal, and this exerts a positive effect only on the ASA_L. The present study shows that the net effect on the ASA_L is positive, and the large increase in ASA_L may cause the large enhancement in RT hydrogen uptake at 6.9 MPa from 2.6 to 4.7 wt %.

We will now further discuss the ASA arising only from the inclusion defects in the cavities (defined as ASA_D). The concentration of the inclusion defects expectedly increases from the M_SC1 to M_SC3 samples. The single-crystal XRD pattern of the imperfect MOF-5 showed the presence of Zn−O, oxygen species, etc. in the nanopores.[15] Our other XRD experiment found that some of the species in the nanopores could not be removed in the degassing process above 200 °C, presumably because certain oxygen species bound strongly to the coordinatively unsaturated Zn at the lattice corner.[1h,i] Therefore, we speculate that the inclusion defects containing the strongly bound oxygen species may increase the ASA_D, which cannot be quantitatively estimated. We suggest future studies of the role of the oxygen species in the nanopores on the RT adsorption of hydrogen via spillover.

The slow kinetics of adsorption (Figure 2) indicate that it is the rate-determining step,[8] which is related to the surface diffusion of atomic hydrogen. Our SAXS study[14] shows that all of the prepared IRMOF-8 samples have a 3-D pore network formed by the aggregation of mesopores as well as micropores. The dense pore

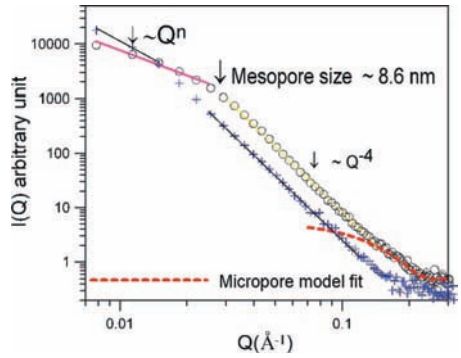

Figure 4. SAXS profiles for the prepared M_SC1 (circles) and M_SC3 (crosses) IRMOF-8 crystals, showing power-law scattering with fractal-like network characteristics in the Q region (0.008∼0.12 $Å^{-1}$) as well as the existence of micropores in the high-Q region.

network of many branches displays the characteristics of self-similarity to some extent (scale). The degrees of density and resultant branches of the pore network progressively increase from M_SC1 to M_SC3, as indicated by the increase in the slope associated with the power-law scattering in the low-Q region of the SAXS profiles (Figure 4)[17](Supporting Information). The formation of the pore network by the aggregation of micropores occurs concurrently with the development of the lattice defects, as shown by the previously combined XRD and SAXS work.[14] It might be inferred that mesoscale (>2 nm) pore channel networks distributed along the dense lattice defects (collapsed framework) have laterally narrow branches (down to the atomic hydrogen scale) that penetrate the boundaries and connect the isolated subgrain-like regions with high ASA_L values.

Bridged M_SC1 IFMOF-8 crystals produced using commercial 10 wt % Pt/C (E-TEK, Inc.) and 40 wt % Pt/C (Johnson Matthey, Co.) as supported catalysts are denoted as M_ET and M_JM, respectively. All of the bridged samples used here have the same Pt content. The M_ET and M_JM samples have almost the same hydrogen uptake of 1.8 wt %, as shown in Figure 1. Their enhancement factors are lower than those of the M_SC samples, due to the effect of carbon-supported catalyst. The enhancement factor is defined as the ratio of the adsorbed amount of the bridged IRMOF-8 via spillover to that of the receptor alone.

The SAXS contributed purely from the pure Pt particles and carbon can be resolved from the ASAXS profiles of the carbon-supported catalysts (Supporting Information). The radii of the Pt particles for 5 wt % Pt/AC (SC) were determined to be ∼27.7 and ∼2.1 nm (bimodal size) by spherical form factor model fitting.[10c−e,14] The radii of the Pt particles for 10 wt % Pt/C (E-TEK) and 40 wt % Pt/C (JM), determined by SAXS analysis, were 1.6 and 2.4 nm, respectively. The carbon black (E-TEK, with a measured BET SSA of ∼200 m^2/g) has a smooth surface.[10a,b] The active carbon (SC, with a measured BET SSA of ∼1000 m^2/g) additionally consists of a dense branch (fractal-like) network of nanopore channels (∼1.4 nm in width), which is evidenced by the power-law characteristics of the SAXS profile and has been described in the literature.[17c] This result suggests that the porous carbon support with high SSA has an open pore channel network, thereby providing more sites and effective pathways for the migration of spiltover hydrogen atoms to the IRMOF-8 and hence leading to higher hydrogen uptake than the usual carbon black. Surprisingly, our experimental results indicate that the size of the Pt particles as a source of atomic hydrogen by dissociation played a minor role in the spillover.

The forms of the H atoms in the lattice and the true way of their migration on the MOF surface remain unknown, based on the current studies.[7b] In conclusion, the optimization of the structures of the imperfect lattice and pore network can significantly facilitate the spillover and thus enhance the RT hydrogen uptake at moderate pressures, up to an amount of full coverage of hydrogen in the MOF (i.e., theoretical maximum storage), regardless of the total SSA value and micropore volume. Our results suggests that a further enhancement in RT hydrogen storage via bridged spillover not only depends on the development of new MOF materials but also on the control of the lattice defects and pore network structure associated with the MOF crystal, which can be optimized by synthesis conditions.

Acknowledgment. We thank M.A. Miller (SwRI, USA) for collaboration on the hydrogen storage measurement.

Supporting Information Available: Experimental details, ASAXS and SAXS profile data, and a detailed discussion. This material is available free of charge via the Internet at http://pubs.acs.org.

References

(1) (a) Yaghi, O. M.; O'Keeffe, M.; Ockwig, N. W.; Chae, H. K.; Eddaoudi, M.; Kim, J. *Nature* **2003**, *423*, 705–714. (b) Eddaoudi, M.; Kim, J.; Rosi, N.; Vodak, D.; Wachter, J.; O'Keeffe, M.; Yaghi, O. M. *Science* **2002**, *295*, 469–472. (c) Chae, H. K.; Siberio-perez, D. Y.; Kim, J.; Go, Y.-B.; Eddaoudi, M.; Matzger, A. J.; O'Keefe, M.; Yaghi, O. M. *Nature* **2004**, *427*, 523–527. (d) Pan, L.; Sander, M. B.; Huang, X.; Li, J.; Smith, M.; Bittner, E.; Bockrath, B.; Johnson, J. K. *J. Am. Chem. Soc.* **2004**, *126*, 1308–1309. (e) Dybtsev, D. N.; Chun, H.; Yoon, S. H.; Kim, D.; Kim, K. *J. Am. Chem. Soc.* **2004**, *126*, 32–33. (f) Eddaoudi, M.; Li, H.; Yaghi, O. M. *J. Am. Chem. Soc.* **2000**, *122*, 1391–1397. (g) Li, H.; Eddaoudi, M.; Groy, T. L.; Yaghi, O. M. *J. Am. Chem. Soc.* **1998**, *120*, 8571–8572. (h) Li, H.; Davis, C. E.; Groy, T. L.; Kelley, D. G.; Yaghi, O. M. *J. Am. Chem. Soc.* **1998**, *120*, 2186–2187. (i) Huang, L.; Wang, H.; Chen, J.; Wang, Z.; Sun, J.; Zhao, D.; Yan, Y. *Microporous Mesoporous Mater.* **2003**, *58*, 105–114.

(2) (a) Rowsell, J. L. C.; Millward, A. R.; Park, K. S.; Yaghi, O. M. *J. Am. Chem. Soc.* **2004**, *126*, 5666–5667. (b) Rowsell, J. L. C.; Eckert, J.; Yaghi, O. M. *J. Am. Chem. Soc.* **2005**, *127*, 14904–14910.

(3) Panella, B.; Hirscher, M.; Pütter, H.; Müller, U. *Adv. Funct. Mater.* **2006**, *16*, 520–524.

(4) Li, Y; Yang, R. T. *J. Am. Chem. Soc.* **2006**, *128*, 726–727.

(5) Li, Y; Yang, R. T. *J. Am. Chem. Soc.* **2006**, *128*, 8136–8137.

(6) Lachawiec, A. J.; Qi, G.; Yang, R. T. *Langmuir* **2005**, *21*, 11418–11424.

(7) (a) Chen, L.; Copper, A. C.; Pez, G. P.; Cheng, H. *J. Phys. Chem. C* **2007**, *111*, 18995–19000. (b) Sha, X.; Knippenberg, T.; Cooper, A. C.; Pez, G. P.; Cheng, H. *J. Phys. Chem. C* **2008**, *112*, 17465–17470.

(8) Li, Y.; Yang, F. H.; Yang, R. T. *J. Phys. Chem. C* **2007**, *111*, 3405–3411.

(9) (a) Li, Y.; Yang, R. T.; Liu, C. J.; Wang, Z. *Ind. Eng. Chem. Res.* **2007**, *46*, 8277–8281. (b) Li, Y.; Yang, R. T. *J. Phys. Chem. C* **2007**, *111*, 11086–11094.

(10) (a) Haubold, H. G.; Wang, X. H.; Goerigk, G.; Schilling, W. *J. Appl. Crystallogr.* **1997**, *30*, 653–658. (b) Jeng, U. S.; Lai, Y. H.; Sheu, H. S.; Lee, J. F.; Sun, Y. S.; Chuang, W. T.; Huang, Y. S.; Liu, D. G. *J. Appl. Crystallogr.* **2007**, *40*, s418–s422. (c) Glatter, O.; Kratky, O. *Small-Angle X-Ray Scattering;* Academic Press: London, 1982. (d) Tsao, C. S.; Chen, C. Y.; Huang, J. Y. *Phys. Rev. B* **2004**, *70*, 174104. (e) Tsao, C.-S.; Chen, H.-L. *Macromolecules* **2004**, *37*, 8984–8991.

(11) Yaghi, O. M.; Eddaoudi, M.; Li, H.; Kim, J.; Rosi, N. U.S. Patent No. 6,930,193 B2, 2005.

(12) (a) Miller, M. A.; Page, R. A. National Testing Laboratory for Solid-State Hydrogen Storage Technologies, US DOE Annual Merit Review Meeting, STP 34, May 18, 2006. (b) Miller, M. A.; Page, R. A. Annual Progress report, DOE Hydrogen Program, Section IV.F.3, FY 2007.

(13) Yang, R. T.; Li, Y.; Lachawiec, A. Annual Progress report, DOE Hydrogen Program, Section J. IV.C.1b, FY 2007.

(14) Tsao, C. S.; Yu, M. S.; Chung, T. Y.; Wu, H. C.; Wang, C. Y.; Chang, K. S.; Chen, H. L. *J. Am. Chem. Soc.* **2007**, *129*, 15997–16004.

(15) Hafizovic, J.; Bjørgen, M.; Olsbye, U.; Dietzel, P. D. C.; Bordiga, S.; Prestipino, C.; Lamberti, C.; Lillerud, K. P. *J. Am. Chem. Soc.* **2007**, *129*, 3612–3620.

(16) (a) Walton, K. S.; Snurr, R. Q. *J. Am. Chem. Soc.* **2007**, *129*, 8552–8556. (b) Düren, T.; Millange, F.; Férey, G.; Walton, K. S.; Snurr, R. Q. *J. Phys. Chem. C* **2007**, *111*, 15350–15356.

(17) (a) Emmerling, A.; Fricke, J. *J. Non-Cryst. Solids* **1992**, *145*, 113–120. (b) Schaefer, D. W. *Science* **1989**, *243*, 1023–1027. (c) Pfeifer, P.; Ehrburger-Dolle, F.; Rieker, T. P.; Gonzalez, M. T.; Hoffman, W. P.; Molina-Sabio, M.; Rodriguez-Reinoso, F.; Schmidt, P. W.; Voss, D. J. *Phys. Rev. Lett.* **2002**, *88*, 115502.

JA802741B